PCCP

Accepted Manuscript

ROYAL SOCIETY OF CHEMISTRY

rsc.li/pccp

View Article Online
DOI: 10.1039/C9CP00451C

Journal Name

ARTICLE

Excitation of singlet-triplet coherences in pairs of nearly-equivalent spins

Received 00th January 20xx,
Accepted 00th January 20xx

DOI: 10.1039/x0xx00000x

www.rsc.org/

Kirill. F. Sheberstov*[a,b], Alexey S Kiryutin[a,c], Christian Bengs[d], Joseph T. Hill-Cousins[d], Lynda J. Brown[d], Richard C. D. Brown[d], Giuseppe Pileio[d], Malcolm H. Levitt[d], Alexandra V. Yurkovskaya[a,c], and Konstantin L. Ivanov*[a,c]

We present approaches for an efficient excitation of singlet-triplet coherences in pairs of nearly-equivalent spins. Standard Nuclear Magnetic Resonance (NMR) pulse sequences do not excite these coherences at all or with very low efficiency. The single quantum singlet-triplet coherences, here termed the outer singlet-triplet coherences, correspond to lines of low intensity in the NMR spectrum of a strongly-coupled spin pair (they are sometimes referred to as "forbidden transitions"), whereas the zero-quantum coherences, here termed the inner singlet-triplet coherences, do not have a direct spectral manifestation. In the present study, we investigated singlet-triplet coherences in a pair of nearly-equivalent carbon spins of the ^{13}C-isotopomer of a specially designed naphthalene derivative with optimized relaxation properties. We propose and compare several techniques to drive the singlet-triplet coherence in strongly coupled spin pairs. First, we study different methods for efficient excitation of the outer singlet-triplet coherences. The achieved conversion efficiency of magnetization to the coherences of interest is close to the theoretically allowed maximum. Second, we propose methods to convert the outer coherences into the inner singlet-triplet coherence. The inner singlet-triplet coherence is insensitive to field inhomogeneity and can be long-lived. By probing this coherence, we perform a very precise measurement of the spin-spin *J*-couplings. A remarkable property of this coherence is that it can be preserved even in absence of a spin-locking radiofrequency field. Consequently, it is possible to shuttle the sample between different magnetic fields preserving the coherence. This allows one to study the field dependence of the relaxation time, T_{IST}, of the inner singlet-triplet coherence by performing field-cycling experiments. We observed dramatic changes of the ratio T_{IST}/T_1 from about 1 (in strong fields) up to 2.4 (in weak fields), which is the evidence of a significant influence of the chemical shift anisotropy on relaxation. We have detected a remarkably long lifetime of the inner singlet-triplet coherence of about 200 s at the magnetic field of 5 mT.

1 Introduction

Long-lived spin order is an important emerging concept in nuclear magnetic resonance (NMR) which holds promise for overcoming some of the limitations imposed by finite spin relaxation times. Long-lived states (LLSs) exist when the static Hamiltonian and the fluctuating Hamiltonian (which causes relaxation) exhibit symmetry relations such that certain states become immune to specific kinds of relaxation[1-4]. A standard example of an LLS is given by the singlet state of a pair of spins that relax predominantly due to the intra-pair dipolar coupling. Singlet order can have much longer lifetime than the longitudinal relaxation time T_1. By exploiting LLSs one can store nuclear spin hyperpolarization[5-8], probe slow molecular dynamics[9, 10] and slow transport[11, 12], and investigate weak ligand-to-protein binding[13, 14]. It is also possible to excite coherences between the singlet and triplet states; some of these coherences demonstrate significantly extended lifetimes[15-18], allowing one to achieve extremely high spectral resolution even in inhomogeneous external fields. By probing such coherences one can measure the spin-spin *J*-couplings with high accuracy of *ca.* 1 mHz, and, consequently, to extract information about conformation or chemical environment of the molecule under the study[15]. It has also been demonstrated that these coherences can be used to measure small residual dipole-dipole couplings in partially aligned media[19].

To generate the singlet order and/or singlet-triplet coherences from equilibrium spin magnetization (and to convert it back into magnetization for NMR detection) one needs to run experiments in a symmetry-broken state of the spin pair rendering the spins chemically or magnetically inequivalent. At the same time, for maintaining the singlet

[a] International Tomography Center, Siberian Branch of the Russian Academy of Science, Novosibirsk, 630090, Russia
[b] Johannes Gutenberg-Universität, Mainz, 55099, Germany
[c] Novosibirsk State University, Novosibirsk, 630090, Russia
[d] School of Chemistry, University of Southampton, Southampton, SO17 1BJ, UK

† Electronic Supplementary Information (ESI) available: [details of any supplementary information available should be included here]. See DOI: 10.1039/x0xx00000x

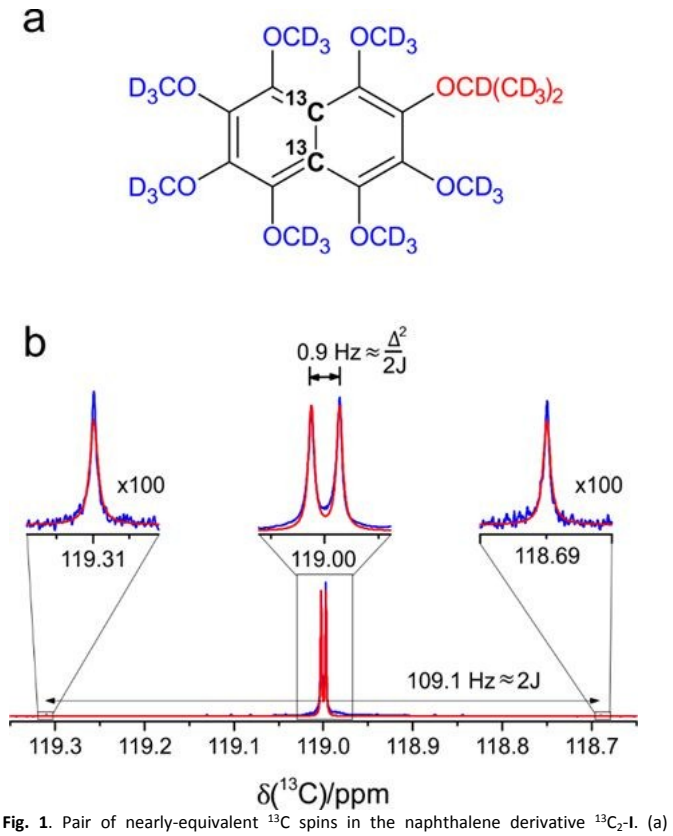

Fig. 1. Pair of nearly-equivalent ^{13}C spins in the naphthalene derivative $^{13}C_2$-**I**. (a) structure of the $^{13}C_2$-**I**. (b) ^{13}C NMR spectrum of $^{13}C_2$-**I** taken at $B_0 = 16.4$ Tesla. (Blue) experimental spectrum obtained after 128 acquisitions, (Red) simulated spectrum with $J = 54.1$ and $\Delta = 10.0$ Hz, the full width at half height (FWHH) is 0.2 Hz. The central lines on the expanded scale and the side signals multiplied by 100 are shown in insets.

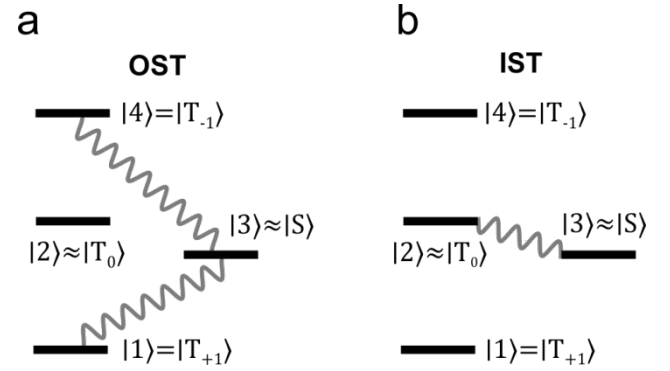

Fig. 2. Energy level diagram of a pair of nearly-equivalent spins. Representation of (a) the OST coherences and (b) the IST coherence, studied in this work (the coherences are denoted by wavy lines).

order, one should impose the symmetry either by transferring the sample to a weak magnetic field or by applying a strong spin-locking RF-field to suppress the evolution under an asymmetric coherent Hamiltonian. In this context, of particular interest are pairs of nearly-equivalent spins, in which the magnitude of scalar coupling, $|J|$, is much greater than the difference in their NMR frequencies, Δ. In such spin pairs the singlet LLS can be maintained at the high external field of an NMR spectrometer even without any manipulations[20-23]. This simplifies the experimental procedures, since there is no need for field-cycling devices to transfer sample and there is no problem with unwanted sample heating caused by spin-locking. The condition of chemical near-equivalence is always fulfilled in low-field experiments, but in some biomolecules such as peptides[20] and in specially designed molecules[21, 22] it can be fulfilled even at a high external field.

Fig. 1 presents a naphthalene derivative (hereafter, $^{13}C_2$-**I**) with two nearly-equivalent ^{13}C-spins and its NMR spectrum taken at 16.4 T (Fig 1b). In this molecule, the singlet spin order has an extraordinarily long lifetime ranging from hundreds of seconds at high magnetic fields up to more than 1 hour at weak magnetic fields[21]. In the spectrum, there are two intense central lines, which can be seen if the spectral resolution is better than 1 Hz, and two outer lines with the frequency difference between them of approximately $2J$. Each of the central lines is approximately 120 times stronger than the outer lines at this magnetic field.

The energy level diagram of a pair of nearly-equivalent spins is presented in Fig. 2. The lowest level $|1\rangle$ corresponds to the state $|T_{+1}\rangle = |\alpha\alpha\rangle$, and the highest level $|4\rangle$ corresponds to the $|T_{-1}\rangle = |\beta\beta\rangle$ state. Hereafter, $|\alpha\rangle$ and $|\beta\rangle$ are the states of spin ½ with the projection on the external magnetic field equal to $+½$ and $-½$, respectively; $|T_m\rangle$, $m\in\{+1, 0, -1\}$, is the component of the triplet state with the angular momentum $m\hbar$ along the magnetic field. The two central energy states of the system under study almost coincide with the central triplet and singlet states, i.e., $|2\rangle \approx |T_0\rangle$ and $|3\rangle \approx |S\rangle$, where $|T_0\rangle = {}^{1}/_{\sqrt{2}}(|\alpha\beta\rangle + |\beta\alpha\rangle)$ and $|S\rangle = {}^{1}/_{\sqrt{2}}(|\alpha\beta\rangle - |\beta\alpha\rangle)$ is the singlet state. The central lines in the spectrum result from excitation of the coherences between the triplet states ρ_{12} and ρ_{24}, whereas the outer peaks come from the ρ_{13} and ρ_{34} coherences, highlighted in Fig. 2a. It is convenient (albeit inaccurate) to refer to the outer peaks in the spectrum as "forbidden transitions". Here we name the corresponding coherences “outer singlet-triplet” (OST) coherences. In the case of a pair of truly equivalent spins, these coherences cannot be excited, and the NMR spectrum appears as just a single line coming from the two coherences between the triplet states, which give rise to NMR lines exactly at the same frequency.

The spectrum shown on Fig. 1b demonstrates an extremely strong “roof” effect (given by the difference in intensities of the central peaks and outer peaks), which is due to two factors: (i) much higher efficiency of exciting the triplet coherences as compared to the OST spin coherences and (ii) different contribution to the observable transverse spin magnetization from coherences of different kinds. It is not possible to eliminate the latter factor, i.e., the small contribution of the OST coherences to NMR signals; however, the former factor can be eliminated by efficient excitation of the forbidden transitions. To this end, special NMR techniques should be used, which are operative when the singlet-triplet transitions are strongly suppressed. Some of these methods have been established

View Article Online DOI: 10.1039/C9CP00454C

previously for generating singlet spin order, such as the M2S (Magnetization-to-Singlet) pulse sequence[20] and SLIC (Spin-Lock Induced Crossing) method[24, 25]. These methods in principle can be adopted to excite the OST coherences with the same efficiency as the single-quantum coherences between the triplet states. Here we describe and compare different approaches for efficient OST excitation and test them using the spin system of the $^{13}C_2$-**I** compound.

In addition to the OST coherences, there is one more singlet-triplet coherence, ρ_{23}, depicted in Fig. 2b, which we name the "inner singlet-triplet" (IST) coherence. This coherence has no direct NMR spectral manifestation; an important property of the IST coherence is that it can be long-lived. Indeed, the splitting between the energy levels $|2\rangle$ and $|3\rangle$ is approximately equal to $|J|$; hence the IST evolution frequency has only a weak dependence on the external magnetic field strength in the case $|\Delta| \ll |J|$, i.e., the frequency is almost insensitive to field inhomogeneity. Furthermore, the contribution of the in-pair dipole-dipole interaction to relaxation of this zero-quantum coherence is reduced as compared to the contribution to the transverse relaxation (i.e., T_2-relaxation) of the single-quantum coherences. For these two reasons, the IST coherence potentially has a long lifetime and is therefore termed a long-lived coherence (LLC)[16-18]. More specifically, it has been shown that for a system of two spins, which relax solely due to mutual dipolar coupling, the LLC lifetime ranges from $3T_2$ to $9T_2$ depending on the motional regime[16], where T_2 is the transverse relaxation time constant. In the extreme narrowing limit the transverse relaxation rate equals the longitudinal one and the LLC lifetime can reach up to $3T_1$. Therefore, one can obtain narrow lines and measure the *J*-coupling with extremely high precision by detecting the IST coherence[15]. However, as mentioned above, the IST coherence cannot be excited and directly observed in simple single-pulse NMR experiments; consequently, special schemes are required for indirect detection of the IST coherence.

We show in this paper that the methods for efficient excitation of the OST coherences in pairs of nearly-equivalent spins can be used as building blocks for more complex pulse sequences designed to excite and probe the IST evolution. We present two pulse sequences of this kind. The first one is related to an approach suggested earlier for probing the LLC in weakly coupled spin pairs[18] in the presence of a spin-locking field. The second pulse sequence exploits the possibility to maintain the IST coherence in strongly-coupled spin pairs without spin-locking at a high field. Moreover, as the IST frequency is almost independent of the external magnetic field strength, this technique is compatible with field-cycling NMR experiments. We demonstrate this experimentally and reveal the field dependence of the relaxation time of the IST coherence.

2 Theory

A detailed theoretical treatment of strongly-coupled spin pairs can be found in NMR textbooks[26-28]. Here we provide some formulas relevant for the discussion. The Hamiltonian of the two spins-1/2, a and b, placed in an external B_0 field (parallel to the z-axis) and coupled by a scalar spin-spin interaction is as follows (written in h units):

$$\hat{H}_0 = -\nu_a \hat{I}_{az} - \nu_b \hat{I}_{bz} + J(\hat{\mathbf{I}}_a \cdot \hat{\mathbf{I}}_b) \quad (1)$$

The frequencies ν_a and ν_b are the precession frequencies of the two spins, $\nu_{a,b} = (1 + \delta_{a,b})\gamma_N B_0/2\pi$ with γ_N being the nuclear gyromagnetic ratio and $\delta_{a,b}$ being the chemical shifts. The term $J(\hat{\mathbf{I}}_a \cdot \hat{\mathbf{I}}_b)$ describes the indirect spin-spin interaction in the pair. The Hamiltonian is modified as follows in the frame rotating at the frequency $\nu_0 = \frac{1}{2}(\nu_a + \nu_b)$, which is the mean value of the chemical shifts of the spin pair:

$$\hat{H}_0 = \frac{\Delta}{2}(\hat{I}_{az} - \hat{I}_{bz}) + J(\hat{\mathbf{I}}_a \cdot \hat{\mathbf{I}}_b), \quad (2)$$

where $\Delta = (\nu_b - \nu_a)$. The eigenstates of this Hamiltonian in terms of the Zeeman states:

$$|1\rangle = |\alpha\alpha\rangle,$$

$$|2\rangle = \cos\tfrac{\theta}{2}|\alpha\beta\rangle + \sin\tfrac{\theta}{2}|\beta\alpha\rangle,$$

$$|3\rangle = \sin\tfrac{\theta}{2}|\alpha\beta\rangle - \cos\tfrac{\theta}{2}|\beta\alpha\rangle,$$

$$|4\rangle = |\beta\beta\rangle, \quad (3)$$

where θ denotes a "mixing angle" of the spin pair, defined here as:

$$\tan\theta = \frac{J}{\Delta} \quad (4)$$

The corresponding eigenvalues, i.e., the state energies, are:

$$E_1 = \frac{J}{4},\ E_2 = -\frac{J}{4} + \frac{1}{2}\sqrt{\Delta^2 + J^2},$$

$$E_3 = -\frac{J}{4} - \frac{1}{2}\sqrt{\Delta^2 + J^2},\ E_4 = \frac{J}{4} \quad (5)$$

In the chosen reference frame the states $|1\rangle$ and $|4\rangle$ are degenerate.

As mentioned in the introduction, for a nearly-equivalent spin pair Δ is much smaller than J, $|\theta| \to \frac{\pi}{2}$ and the eigenstates $|2\rangle$ and $|3\rangle$ almost exactly coincide with the $|T_0\rangle$ and $|S\rangle$ states, respectively. Let us introduce a ratio of matrix elements χ defined as:

$$\chi = \frac{\langle 2|\hat{I}_x|1\rangle}{\langle 3|\hat{I}_x|1\rangle} = \frac{\cos^{\theta}/_2 + \sin^{\theta}/_2}{\cos^{\theta}/_2 - \sin^{\theta}/_2} \quad (6)$$

The ratio of the inner to the outer line intensities equals to χ^2, and for the system under study it is approximately 120 (as obtained using $\Delta = 10$ Hz at $B_0 = 16.4$ T and $J = 54.1$ Hz).

The application of a hard $\frac{\pi}{2}$-pulse to a system of spins at equilibrium conditions with z-polarization (Fig. 3a) efficiently excites the coherences ρ_{12} and ρ_{24} between the triplet states

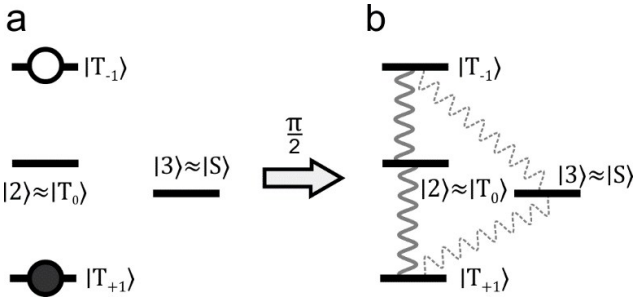

Fig. 3. Diagram, representing the action of a $\frac{\pi}{2}$-pulse on a pair of nearly-equivalent spins. (a) Initial equilibrium state of the spin system polarized along z-axis, the $|T_{+1}\rangle$ state is over-populated whereas the $|T_{-1}\rangle$ state is under-populated with respect to the $|T_0\rangle$ and $|S\rangle$ states. (b) Excitation of the single quantum coherences by applying the pulse. Upon NMR excitation, the coherences within the triplet manifold have χ times larger amplitudes than the OST coherences.

with the amplitudes proportional to $\langle 2 | \hat{I}_x | 1 \rangle$, whereas the OST coherences are excited inefficiently and their amplitudes are proportional to $\langle 3 | \hat{I}_x | 1 \rangle$ (Fig. 3b). NMR detection further scales down the relative intensities of the outer peaks to the central peaks by a factor of χ.

2.1 Methods for efficient excitation of the OST coherences

We exploit and compare several approaches for efficient excitation of the OST coherences in nearly-equivalent spin pairs. A clear indication of efficient excitation of the OST coherences is the enhancement of the outer NMR lines corresponding to the "forbidden" transitions. The maximal achievable enhancement of two OST coherences can be derived using unitary bounds for spin dynamics[29, 30]; the maximal enhancement factor is equal to χ (see ESI†).

The methods for efficient excitation of OST transitions are outlined in Fig. 4. First, we use techniques that are based on simultaneous excitation of the OST transitions by weak selective amplitude-modulated (AM) RF-pulses (Fig. 4a and 4b). Second, we implement the SLIC method[24], which exploits a resonant RF-field applied at the ν_0 frequency with a pulse amplitude, B_1, is set such that the nutation frequency ν_1 matches the J-coupling (Fig. 4d). Third, we demonstrate excitation of singlet-triplet transitions using a Carr-Purcell-Meiboom-Gill (CPMG) sequence[31, 32] with a special choice of inter-pulse intervals synchronized with the J-coupling driven evolution (Fig. 4e). Composite pulses can be used for 180 rotations[33], which are more robust in case of inhomogeneous B_1 fields. Such a J-CPMG sequence has been used as a component of the M2S and S2M schemes for generating the population differences between the singlet and triplet state [20].

2.1.1 Simultaneous selective excitation of the OST coherences by rectangular AM pulses

The first method we consider here is based on simultaneous selective excitation of the two OST transitions. Simultaneous irradiation at two frequencies can be achieved by introducing amplitude modulation to an RF pulse. Let us consider such an AM rectangular pulse (Fig. 4a), which is given

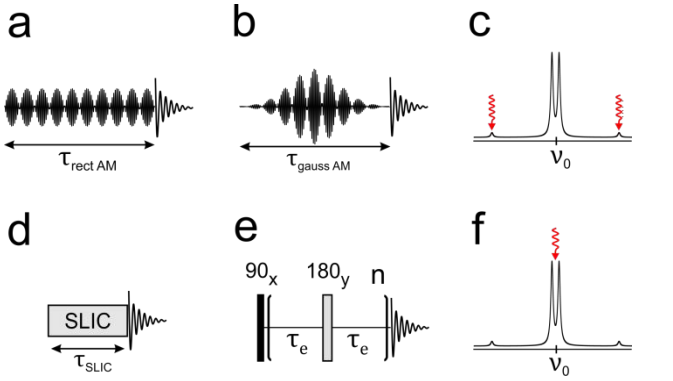

Fig. 4. Techniques for enhancing the OST coherences: (a) simultaneous selective excitation using an amplitude modulated rectangular pulse; (b) the same experiment using a Gaussian pulse shape; (c) NMR spectrum of a strongly coupled spin pair with the frequency positions indicated, at which the selective pulses are applied for the schemes (a) and (b). (d) Application of a single SLIC-pulse, the pulse amplitude is set such that the nutation frequency ν_1 matches the J-coupling. (e) Adaptation of the CPMG pulse sequence, the echo delay τ_e should be equal to $\approx (4J)^{-1}$ for a strongly coupled spin pair. (f) NMR spectrum of a strongly coupled spin pair with the frequency position indicated, at which the SLIC-pulse is applied. After application of the pulse sequence the Free Induction Decay (FID) signal is detected; its Fourier transform gives the NMR spectrum.

by a time-dependent RF-field:

$$B_1(t) = B_1 \cos(2\pi\nu_{rf}t)\cos(2\pi\nu_{AM}t - \phi_{AM}) \quad (7)$$

The phase shift ϕ_{AM} in the amplitude modulation is not important for calculations of the efficiency of the OST coherences; for the sake of simplicity, we set it equal to zero. Using the product-to-sum trigonometric identity it can be shown that the AM pulse given in eq. 7 is equivalent to irradiation at two frequencies around the transmitter frequency, ν_{rf}, with two times weaker RF-field amplitude:

$$B_1(t) = \frac{B_1}{2}[\cos(2\pi\nu_{rf}t + 2\pi\nu_{AM}t) + \cos(2\pi\nu_{rf}t - 2\pi\nu_{AM}t)] \quad (8)$$

In order to irradiate the OST transitions as shown on Fig. 4c, the frequency of the transmitter is set equal to the ν_0 frequency, and the ν_{AM} frequency should be set equal to half of the splitting between the outer peaks:

$$\nu_{AM} = \frac{J + \sqrt{J^2 + \Delta^2}}{2} \approx J + \frac{\Delta^2}{4J} \quad (9)$$

In general, the AM pulse needs to be selective enough so that is does not affect the central transitions. This requires the condition $\nu_1 \ll \nu_{AM}$, where the spin nutation frequency under the action of the pulse is determined as

$$\nu_1 = \gamma_N B_1 / 2\pi \quad (10)$$

In the present case, it is impossible to select a reference frame such that the Hamiltonian is time-independent, instead it

Journal Name ARTICLE

is periodic: once we write down the Hamiltonian in the frame rotating at the ν_0 frequency, it contains oscillatory terms with the oscillation frequency being equal to ν_{AM}. One of the possible ways to find analytical expressions for the excitation efficiency under a periodic perturbation is to exploit the Floquet theory, which is a commonly used approach in solid-state NMR[34], as well as in some solution-state applications[35]. In this approach, the Hamiltonian is expanded into a Fourier series, the time-independent coefficients of this expansion are then used to construct the Floquet Hamiltonian. In the case under consideration there is a single characteristic frequency ν_{AM}, so there is a limited number of non-zero elements in the Floquet Hamiltonian. Here we do not present a detailed evaluation but discuss some intermediate steps and results. The present case is very similar to that of simultaneous excitation of the two single-quantum transitions in a spin-1 system, as the two transitions share a common energy level $|3\rangle$. The Floquet Hamiltonian has been previously expressed for a spin-1 system under double frequency irradiation[36], so we adopted the known results. When constructing the Floquet Hamiltonian, it is convenient to split the Hamiltonian into a time-independent term (which appears at the diagonal blocks of the Floquet Hamiltonian) and a periodic term (appearing at non-diagonal blocks of the Floquet Hamiltonian). It is convenient to choose a frame rotating at the frequency ν_0 with the static Hamiltonian given in eq. 2. It can be rewritten in terms of fictitious spin-1/2 operators[37] as:

$$\hat{H}_0 = \frac{J}{2}\hat{I}_z^{12} - \frac{J}{2}\hat{I}_z^{34} + \sqrt{J^2+\Delta^2}\,\hat{I}_z^{23} \qquad (11)$$

where $\hat{I}_\alpha^{ij}$ is a fictitious spin operator between eigenstates $|i\rangle$ and $|j\rangle$ defined in eq. 3 along the $\alpha\in(x,y,z)$ axis. The periodic Hamiltonian of the cosine-modulated rectangular pulse can be written as follows:

$$\hat{H}_1(t) = \nu_1 \cos(2\pi\nu_{AM}t)\left[\left(\cos{}^{\theta}\!/_{2} + \sin{}^{\theta}\!/_{2}\right)\left(\hat{I}_x^{12}+\hat{I}_x^{24}\right) + \left(\cos{}^{\theta}\!/_{2} - \sin{}^{\theta}\!/_{2}\right)\left(\hat{I}_x^{13}+\hat{I}_x^{34}\right)\right] \qquad (12)$$

Using eqs. 11 and 12 it is straightforward to construct the Floquet Hamiltonian, which is very similar to that presented in Ref.[36]. Eq. 9 is essentially a resonance condition, at which the Floquet Hamiltonian has level anti-crossings, and the non-diagonal elements appear in their full form in an effective Hamiltonian (which is sometimes also called "stroboscopic"); in the present case this Hamiltonian is given by expression:

$$\hat{H}_{eff} = \frac{\nu_1}{2}\left(\cos{}^{\theta}\!/_{2} - \sin{}^{\theta}\!/_{2}\right)\left(\hat{I}_x^{13}+\hat{I}_x^{34}\right) \qquad (13)$$

The initial equilibrium state is proportional to $\left(\hat{I}_z^{13}+\hat{I}_z^{34}\right)$ and it evolves under the action of the effective Hamiltonian according to the following equation:

$$\hat{\rho}(t) = e^{-2\pi i t\,\hat{H}_{eff}}\left(\hat{I}_z^{13}+\hat{I}_z^{34}\right)e^{2\pi i t\,\hat{H}_{eff}} \qquad (14)$$

It is possible to find analytical solution for $\hat{\rho}(t)$:

$$\hat{\rho}(t) = \cos[2\pi\nu_{eff}t]\left(\hat{I}_z^{13}+\hat{I}_z^{34}\right) - \frac{1}{\sqrt{2}}\sin[2\pi\nu_{eff}t]\left(\hat{I}_y^{13}+\hat{I}_y^{34}\right),$$

$$\nu_{eff} = \frac{\nu_1}{2\sqrt{2}}\left(\cos{}^{\theta}\!/_{2} - \sin{}^{\theta}\!/_{2}\right) \qquad (15)$$

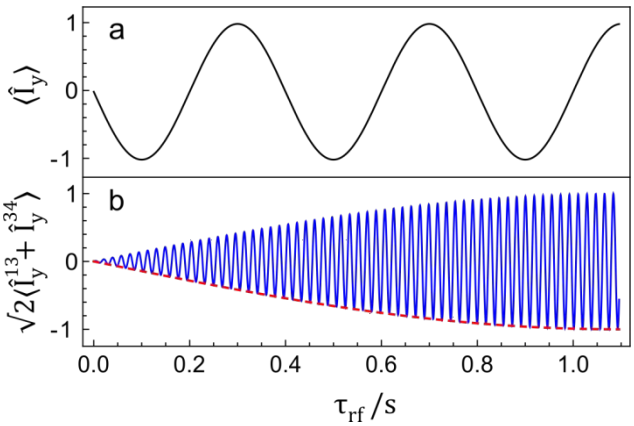

Fig. 5. Simulated trajectories of spin nutation under the action of an RF-pulse. (a) Evolution of the single-quantum coherence of a spin-1/2 particle under the action of a resonant rectangular pulse with the amplitude corresponding to the nutation frequency $\nu_1 = 2.5$ Hz. (b) Evolution of the OST coherences under the action of an AM rectangular pulse. The solid line corresponds to numerical calculations of the evolution under the static Hamiltonian given by eq. 2 together with the pulse given in eq. 12. The dashed line corresponds to the evolution under the effective Hamiltonian given in the eq. 13. The following parameters were used in the simulation: $\Delta = 10$ Hz and $J = 54.1$ Hz, $\nu_{AM} = 54.558$ Hz, $\phi_{AM} = 0$, $\nu_1 = 5$ Hz.

This expression is again similar to those describing the excitation of single-quantum coherences in a spin-1 particle.

Fig. 5 presents the results of numerical simulations of the evolution of different coherences under RF-pulses. First, spin nutation is shown for the "usual" single-quantum coherence (e.g. for the transverse magnetization of a spin-1/2 particle) around the RF-field with the amplitude, which corresponds to a nutation frequency of 2.5 Hz (Fig. 5a). Second, nutation of the OST coherence under an equivalent AM pulse (it has an amplitude corresponding to a 5 Hz nutation frequency, Fig. 5b) is shown. In the latter case, the same spin system is considered, which is discussed in the introduction: $\Delta = 10$ Hz and $J = 54.1$ Hz. The evolution under the effective Hamiltonian is shown by the dotted red line Fig. 5b, describing the evolution of the amplitude of the OST coherences. The amplitude of the OST coherences thus experiences nutation with the frequency being χ times slower than that of the single-quantum triplet-triplet coherence; in the present case the evolution is approximately 10.9 times slower. This finding again reflects the fact that the OST coherences are less efficiently coupled to the NMR coil, consequently they have a lower nutation frequency and also produce a weaker NMR signal. The numerical simulation is shown by the solid blue line in Fig. 5b; it additionally contains a fast oscillating component corresponding to the evolution of the state under the static Hamiltonian. Since these coherences are the coherences between the eigenstates of the static

Hamiltonian $\hat{H}_0$, see eq. 2, they acquire a time-dependent phase shift given by $\exp(-2\pi i \nu_{ij} t)$ with the frequencies of the corresponding energy differences, which are equal to $\nu_{13} = \nu_{34} = \frac{1}{2}(J + \sqrt{J^2 + \Delta^2})$. It can be shown that this oscillation corresponds to the evolution between the $(\hat{I}_y^{13} + \hat{I}_y^{34})$ and $(\hat{I}_x^{13} - \hat{I}_x^{34})$ states.

Thus, the duration of the selective AM pulse for efficient excitation of the OST coherences should be set as follows:

$$\tau_{rect\ AM} = \frac{1}{2\nu_1} \cdot \frac{\sqrt{2}}{\cos \theta/2 - \sin \theta/2} \qquad (16)$$

The first factor of $1/2\nu_1$ corresponds to the duration of a $\frac{\pi}{2}$-pulse with the amplitude corresponding to the nutation frequency of $\frac{\nu_1}{2}$. The second term scales the pulse length required to perform efficient excitation of the OST transitions. Due to scaling, the pulse should be approximately χ times longer in order to completely excite the OST coherences.

2.1.2 Simultaneous selective excitation of the OST coherences by a Gaussian AM pulse

It is possible to improve the selectivity of excitation by applying shaped pulses instead of rectangular pulses, e.g. Gaussian pulses as shown in Fig. 4b. For a Gaussian pulse, the RF-field is as follows:

$$B_1(t) = B_1^{Gauss} \exp\left(-\frac{\ln 2 (t - \tau_p/2)^2}{(\beta \tau_p)^2}\right) \cos(2\pi \nu_{rf} t)$$
$$\cos(2\pi \nu_{AM} t - \phi_{AM}) \qquad (17)$$

Where τ_p corresponds to the total duration of the Gaussian pulse and the β parameter sets the width of the Gaussian envelope. Gaussian pulses enable more narrow-band excitation and excite the central NMR transition to a smaller extent. The spin dynamics under the action of such a shaped pulse is similar to that for the rectangular pulse, but there is an additional calibration step. In order to completely excite the OST coherences by a rectangular pulse, one should use eq. 16 to set the pulse duration for a given RF-pulse amplitude. An equivalent shaped pulse is a pulse with the same integral of the RF-envelope over the same pulse duration. Consequently, the maximal amplitude of the Gaussian pulse should be rescaled relative to the rectangular pulse:

$$B_1^{Gauss} = \frac{B_1^{Rect}}{\beta} \sqrt{\frac{\ln 2}{\pi}} \qquad (18)$$

2.1.3 Excitation of the OST coherences by a SLIC pulse

Implementation of the SLIC-pulse (Fig. 4d) also results in enhancement of the OST transitions, as explained below. In this case, the spin system evolves under the action of the following Hamiltonian (valid when the RF-field is applied at the $\nu_{rf} = \nu_0$ frequency):

$$\hat{H}_{rf} = \frac{\Delta}{2}(\hat{I}_{az} - \hat{I}_{bz}) - \nu_1(\hat{I}_{ax} + \hat{I}_{bx}) + J(\hat{\mathbf{I}}_a \cdot \hat{\mathbf{I}}_b) \qquad (19)$$

For the case considered here (nearly equivalent spins) the small Δ-term can be considered as a perturbation and is neglected in the first step. The eigenvalue problem is then solved for the remaining part of $\hat{H}_{rf}$. The solution provides the singlet and three triplet eigenstates. One should note, however, that the "new" triplet states are those in the "tilted" reference frame with the quantization axis parallel to the

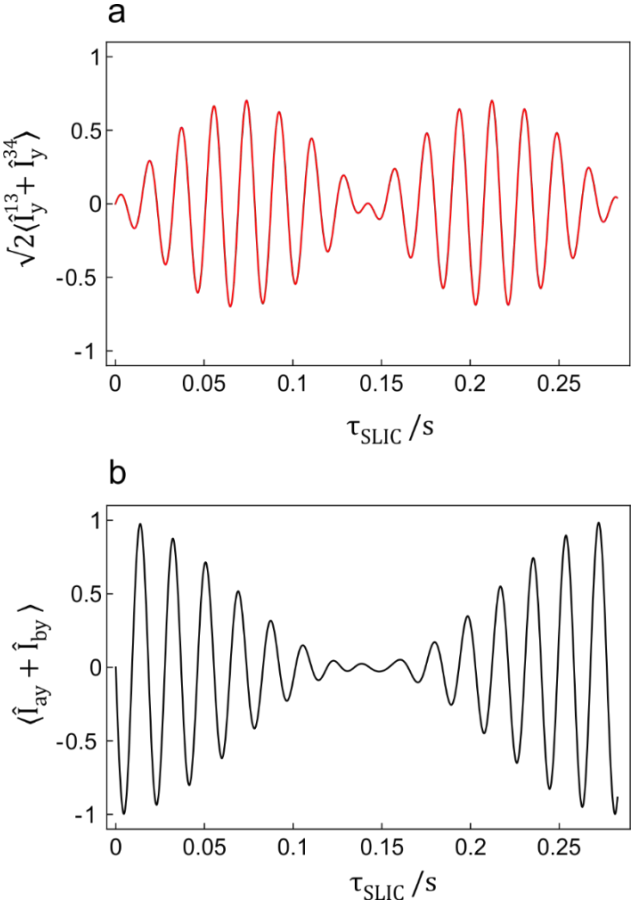

Fig. 6. Simulated trajectories for nutation under a SLIC-pulse. (a) Evolution of the OST coherences (b) Evolution of the y magnetization. The following parameters were used for the simulations: $\Delta = 10$ Hz and $J = 54.1$ Hz, $\nu_1 = 54.1$ Hz.

x-axis. These triplet states are expressed via $|T_0\rangle, |T_{+1}\rangle, |T_{-1}\rangle$ in the following way:

$$|T'_0\rangle = \frac{|T_{+1}\rangle - |T_{-1}\rangle}{\sqrt{2}},$$

$$|T'_{+1}\rangle = \frac{1}{\sqrt{2}}|T_0\rangle + \frac{|T_{+1}\rangle + |T_{-1}\rangle}{2},$$

$$|T'_{-1}\rangle = \frac{1}{\sqrt{2}}|T_0\rangle - \frac{|T_{+1}\rangle + |T_{-1}\rangle}{2} \qquad (20)$$

and their energies are approximately equal to (neglecting Δ):

$$E(T'_0) = \frac{J}{4}, \quad E(T'_{+1}) = \frac{J}{4} + \nu_1, \quad E(T'_{-1}) = \frac{J}{4} - \nu_1 \qquad (21)$$

The energy of the singlet state is equal to

View Article Online
DOI: 10.1039/C9CP00451C

$$E(S) = -\frac{3J}{4} \quad (22)$$

The condition $\nu_1 \approx |J|$ results in a level crossing: $E(S) \approx E(T'_{-1})$, the $|S\rangle$ and $|T'_{-1}\rangle$ states become nearly degenerate and the Δ-term comes into play and mixes the two levels inducing singlet-triplet transitions.

The initial equilibrium state in the eigenbasis eq. 20 is represented as a sum of two coherences: $\rho_{T'_{-1}T'_0}$ and $\rho_{T'_{+1}T'_0}$. Because of the singlet-triplet mixing, the $\rho_{T'_{-1}T'_0}$ coherences gradually evolves into a $\rho_{ST'_0}$ coherence. This coherence

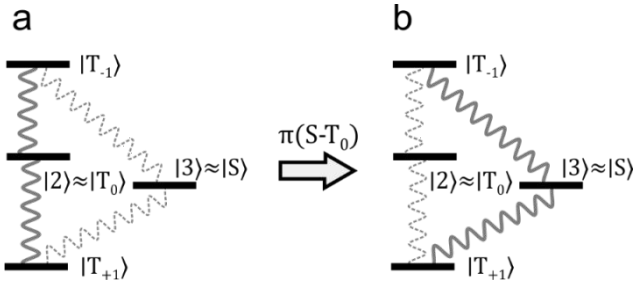

Fig. 7. Diagrams representing the coherences before applying the echo train in the J-CPMG sequence (a) and after applying it (b). The overall effect of the J-CPMG sequence is to swap the initially excited triplet coherences with the OST coherences resulting in enhancement of the OST coherences ρ_{13} and ρ_{34}.

corresponds to the OST coherences ρ_{13} and ρ_{34} in the original eigenbasis, see eq. 3, which is relevant after switching off the SLIC-pulse. The corresponding spin dynamics are illustrated in Fig. 6 with numerical simulations. First, the pulse efficiently drives transitions within the triplet manifold and generates the spin coherences corresponding to the $(\hat{I}_{ay} + \hat{I}_{by})$ spin order (Fig. 6b). The OST coherences are again excited at significantly longer times as compared to the triplet ones (Fig. 6a), and the SLIC-pulse should be applied for $\tau_{SLIC} = \frac{1}{\sqrt{2}\Delta}$ until maximal T'_{-1}-S conversion is reached. The achievable amplitude of the excited OST coherences is, however, a factor of $\sqrt{2}$ smaller than in the case of simultaneous selective excitation. The reason is that the SLIC-pulse not only excites the OST coherences of interest but additionally excites unwanted triplet coherences. Note however, that the duration of the excitation period in the SLIC method is usually shorter than that for AM selective pulses.

2.1.4 Excitation of the OST coherences by J-CPMG

Finally, we propose to use the pulse sequence, which we name J-CPMG (Fig. 4e): this pulse sequence is a part of the original M2S-sequence proposed to manipulate the singlet order in near-equivalent spin pairs[20]. The inter-pulse delay and number of echoes should be set as follows:

$$\tau_e = \frac{1}{4\sqrt{J^2 + \Delta^2}} \approx \frac{1}{4J},$$

$$n = \mathrm{round}\left(\frac{\pi}{\pi - 2\theta}\right) \quad (23)$$

Theoretical treatment of excitation of the OST coherences by the J-CPMG has been presented in the original paper[20]; here we only show the diagram illustrating how the coherences which were initially excited by a $\frac{\pi}{2}$ pulse are transformed by the echo train (Fig. 7). The effect of the echo train is swapping the triplet coherences (excited with high amplitude by the first pulse) with the OST coherences (that are excited very inefficiently). Hence, the final state after applying the J-CPMG sequence is $(\hat{I}_{ax} - \hat{I}_{bx})$, which contains the $(\hat{I}_x^{13} - \hat{I}_x^{34})$ term corresponding to the OST coherences of interest. Generation of this spin order also corresponds to enhancement of the outer NMR lines by a factor of χ.

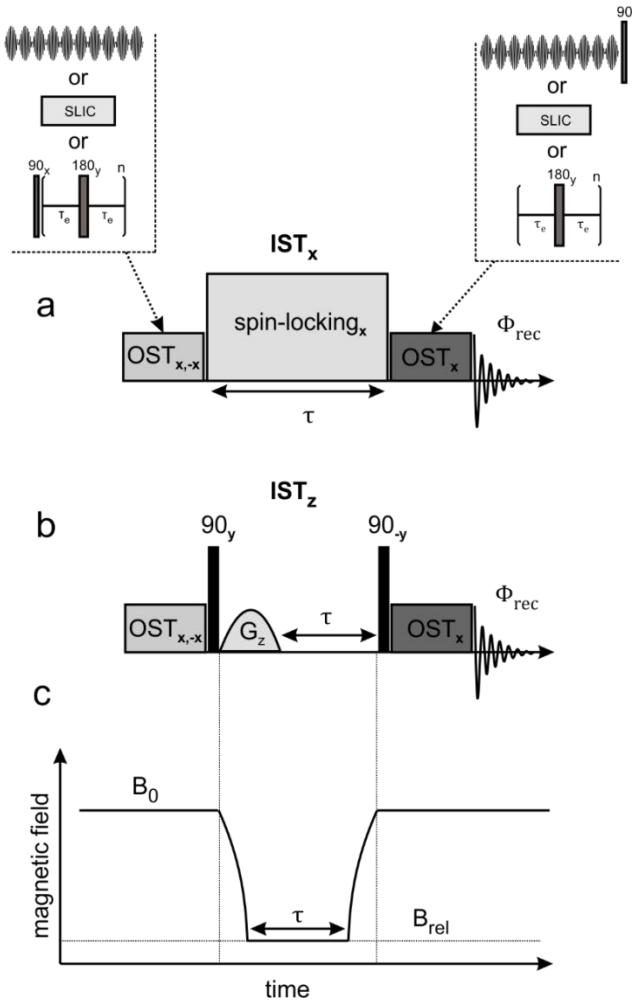

Fig. 8. Pulse sequences for indirect observation of the IST coherence evolution. (a) Method to measure the IST evolution in the rotating reference frame under a spin-locking field. (b) Method to measure the IST evolution in the laboratory reference frame. (c) Variation of the external magnetic field in the field-cycling experiments. G_z stands for a pulsed field gradient parallel to the B_0 magnetic field. OST blocks denote methods for conversion of magnetization into OST coherences, as described in sections 2.1.1–2.1.4. The backwards conversion is slightly different for each method as shown in the inset. The phase cycle of the first OST block and of the receiver, $\Phi_{rec} = y, -y$, can be used to suppress unwanted background signals. The NMR spectrum is obtained as the Fourier transform of the FID signal. The pulse sequences for Bruker spectrometers are available in ESI†.

2.2 Exciting and probing the IST coherence

Here we suggest two approaches for probing the evolution of the IST coherence for nearly-equivalent spins. In both

approaches, the IST coherence is created from the OST coherences, excited by any of the methods described in sections 2.1.1–2.1.4. The IST coherence evolves during a time period of variable duration, τ, and is then converted back into the transverse magnetization for NMR detection. The backward conversion is performed using slightly modified blocks, which are used for OST excitation, and converts the IST coherence into the transverse magnetization. The pulse sequences for experiments with the IST coherence are depicted in Fig. 8. The two approaches differ in the way how the OST coherences are converted into the IST coherence, as described below.

2.2.1 IST coherence in the rotating reference frame

The first approach is presented in Fig. 8a. The experiment starts with excitation of the OST coherences by any of the outlined methods. Application of the excitation block modifies the spin order; the resulting spin order can be written in following general form:

$$\sqrt{2}\sin\varphi\left(\hat{I}_y^{13}+\hat{I}_y^{34}\right)+\sqrt{2}\cos\varphi\left(\hat{I}_x^{13}-\hat{I}_x^{34}\right) \qquad (24)$$

Neglecting the small differences between the energies of the true eigenstates of the spin system, see eq. 3, and the singlet and triplet states, we can rewrite the spin order in the following way:

$$\frac{\exp(-i\varphi)}{\sqrt{2}}\left(|S\rangle\langle T_{+1}|-|S\rangle\langle T_{-1}|\right)+\frac{\exp(i\varphi)}{\sqrt{2}}\left(|T_{+1}\rangle\langle S|-|T_{-1}\rangle\langle S|\right) \qquad (25)$$

As has been described in section 2.1.3, a strong spin-locking RF-field rotates the quantization axis $z\rightarrow x$; the new eigenbasis is then given by eq. 20, so the original $|T_{+1}\rangle$ and $|T_{-1}\rangle$ states are turned into the $|T'_0\rangle$ state by the basis rotation. Then, in the tilted frame, the state eq. 25 is transformed into the following expression:

$$\exp(-i\varphi)|S\rangle\langle T'_0|+\exp(i\varphi)|T'_0\rangle\langle S| \qquad (26)$$

This is a coherence between the eigenstates of the $\hat{H}_{rf}$ Hamiltonian, see eq. 19. The energy gap between the $|S\rangle$ and $|T'_0\rangle$ states equals to the *J*-coupling, see eqs. 21 and 22. Consequently, the IST coherence acquires a time-dependent phase shift with the characteristic frequency of J, which is then readout through the intensity of the central signals after the backward conversion. Note, that the evolution frequency does not depend on the strength of the B_0 magnetic field, as far as the spin-locking field is strong enough, so there is no decay of the coherence due to B_0 field inhomogeneity. Hereafter, we name this type of measurement IST_x, corresponding to the IST coherence in the tilted frame. In the present case, spin-locking also allows one to suppress the coherent singlet-triplet leakage, similar to the previously proposed method for weakly coupled spins[17, 18].

2.2.2 IST coherence in the laboratory reference frame

The second approach exploits the slow coherent singlet-triplet leakage of near-equivalent spins[19-21], allowing to probe the IST coherence even in the absence of spin-locking as it is shown in Fig. 8b. We term this scheme IST_z, corresponding to the IST coherence in the lab frame. Transformation of the OST coherences as described in eq. 24 into the IST coherence is done by a $\frac{\pi}{2}$-pulse having the y-phase, which results in the following coherence:

$$\exp(-i\varphi)|3\rangle\langle 2|+\exp(i\varphi)|2\rangle\langle 3| \qquad (27)$$

This expression corresponds to the IST coherence between the eigenstates of the static Hamiltonian of laboratory frame, see eq. 1, and the oscillation frequency is given by the energy difference for the corresponding eigenstates, see eq. 5, which is equal to $\sqrt{J^2+\Delta^2}$. So in the case of a small chemical shift difference between the spins there is only a minor dependence on the magnetic field B_0. In practice it is possible to use a pulsed field gradient for washing out all coherences except for the IST coherence of interest. This remarkable property of the IST coherence (weak dependence of the oscillation frequency on the B_0 field) also allows one shuttling of the sample between different fields, while the coherence continues to precess with the same frequency so that it is not washed out upon field variation. The change of the external magnetic field during a shuttling experiment is schematically shown in Fig. 8c: immediately after generation of the IST coherence the sample is transferred to the B_{rel} magnetic field, where free evolution of the IST coherence takes place during the period τ; after that the sample is transferred back to the detection field and the FID is acquired after the backward conversion of the IST coherence into spin magnetization.

Therefore, in experiments with the IST coherence we exploit the methods for exciting OST transitions as building blocks. By varying the delay τ one can vary the free evolution time of the IST coherence. In this way, by measuring the resulting signal at variable τ one can assess the IST coherence evolution: the resulting signal plotted as a function of τ contains an oscillatory component, the frequency of oscillations is given by the energy gap between the singlet and triplet states.

3 Experiment

We studied a naphthalene derivative, 1,2,3,4,5,6,8-heptakis([D_3]methoxy)-7-((([D_7]propane-2-yl)oxy)-naphthalene (compound **I**) shown in Fig. 1a and described in ref. [21]. The compound was synthesized as described in ref. [38] and the sample prepared as follows. Solution of $^{13}C_2$-**I** in acetone-d_6 with concentration of 0.02 M was placed in 110 µl cylindrical microcell insert (Wilmad-LabGlass, 529-E), degassed by three freeze–pump–thaw cycles and flame-sealed. The sealed microcell insert was placed into a standard 5 mm NMR tube, and was fixed about 1 cm above the bottom. The NMR tube

View Article Online
DOI: 10.1039/C9CP00451C

(with the insert inside) was filled by protonated acetone and sealed.

The singlet lifetime, T_S, of carbons in $^{13}C_2$-**I** for this sample was 1240 ± 40 s at the B_0 field of 9.4 T. This time is long enough for the molecules to diffuse across the whole sample assuming typical convection rates of *ca.* 0.01 mm/s in NMR measurements[39]. For this reason, it is important to restrict the sample size within the active volume of the NMR coil. Although signal losses are still possible due to the combined effect of the convection together with B_1 inhomogeneity[40], they are not so dramatic, especially for the methods based on composite hard pulses[33]. However, reduction of the sample volume causes problems: it makes significantly harder the procedure of shimming the B_0 homogeneity, and even more important it causes instabilities of the B_0 field, which are observed due to the variable level of the liquid for volatile solvents, which can evaporate and condense on the top of the sample tube. The sample preparation method described here allows one to place the whole sample inside the active volume of the NMR coil and to achieve a highly homogeneous and stable B_0 field.

NMR experiments on excitation of the OST and IST coherences were performed using Bruker NMR spectrometers with the B_0 fields of 9.4 T and 16.4 T, corresponding to 400 MHz and 700 MHz proton Larmor frequency, respectively.

It is possible to set the phase of the amplitude modulation, ϕ_{AM}, for simultaneous selective excitation, which was introduced in eq. 7, in such a way that the OST coherences appear exactly as the $\left(\hat{I}_y^{13} + \hat{I}_y^{34}\right)$ spin order (corresponding to the in-phase appearance of the outer NMR lines). Hence, one can phase the spectra in the same way as conventional 1D NMR spectra (the same relative phases of the pulse and receiver, the same offset, and the delay between pulse and beginning of the FID registration). To do so, one should set the phase according to:

$$\phi_{AM} = 2\pi \cdot \tau_p \cdot \nu_{AM} \qquad (28)$$

Such a phase shift sets the value of the $B_1(\tau_p) = B_1$ giving rise to cosine modulation. The OST coherences evolve at the same ν_{AM} frequency. Amplitude modulation with respect to the pulse end is done using the Shape-tool of the TopSpin software for Bruker spectrometers. Note that in the case of sine modulation with the same ϕ_{AM} phase shift, the OST coherences appear as $\left(\hat{I}_x^{13} - \hat{I}_x^{34}\right)$ spin order (corresponding to an anti-phase doublet of the outer peaks), requiring an additional $\frac{\pi}{2}$ phase shift for phasing.

Here we always used Gaussian pulses with the width parameter from eq. 18 equal to $\beta = 0.194$, which corresponds to a Gaussian shape, perturbed at 1% level as generated in the Shape-tool software.

Experiments with the IST coherence were done with a two-step phase cycle for efficient suppression of NMR signals, which are not encoded by the first OST block (in practice these contributions lead to unwanted background signals). In all experiments, the relaxation period between subsequent experiments was set to $5T_1$. In addition, we exploited a pre-saturation SLIC-pulse of a duration of $3T_1$ before the relaxation delay with the aim to eliminate possible long-lived singlet-triplet population imbalance, which otherwise has a lifetime of T_S.

The 9.4 T spectrometer that we used is equipped with an additional sample shuttling system[41, 42], allowing us perform measurements at low fields, here down to 5 mT. The transfer time was always 0.6 s. The time can be controlled with a precision better than 0.1 ms, which is sufficient to sample the oscillatory behavior of the coherences under the study. In our field-cycling experiments, it is difficult to control the temperature precisely. Since the chemical shifts of ^{13}C-nuclei are sensitive to small temperature variations, in field-cycling experiments we used the J-CPMG method, because it is less sensitive to small chemical shift variations compared to the techniques using selective excitation. Each spectrum was acquired twice: first time with the x phase and second time with the $-x$ phase of the first OST block. The spectra were then integrated and the integral values were subtracted.

4 Data analysis

All obtained spectra were phased as standard 1D NMR spectra acquired with the same relative phases of the pulse and receiver; the same irradiation frequency and the same delay between the pulse and FID acquisition were used, unless otherwise stated. An important technical issue in the experiments on excitation of the OST transitions is setting the integration window in the NMR spectra to improve the signal-to-noise ratio. Here, to minimize the experimental noise we set the integration limits to approximately ± 1.4 FWHH from the center of the peaks[43]. We performed the spin dynamics calculations using SpinDynamica[44] and specified the spin system parameters of $^{13}C_2$-**I** using ANATOLIA[45]. The determined spin system parameters were: $J = 54.1 \pm 0.1$ Hz and $\Delta = 10.0 \pm 0.01$ Hz at 16.4 T with FWHH of the simulated spectrum of 0.23 Hz.

5 Results and discussion

5.1 Enhancement of the OST transitions

We compared the experimental spectra obtained by simultaneous selective excitation, SLIC and J-CPMG methods used for enhancing the OST transitions (Fig. 9). Excitation of these coherences is probed in a straightforward way by measuring the enhancement of the corresponding NMR transitions. In all methods, we observed a significant increase in the intensity of the "forbidden" OST transitions; the enhancement is close to the theoretically allowed maximum value, which is $\varepsilon = \chi \approx 10.9$ for the ^{13}C spin pair of the $^{13}C_2$-**I**

compound. Hence, we are indeed able to achieve efficient excitation of the OST coherences.

The results obtained by simultaneous selective excitation are shown in Fig. 9b and 9c. We have tried rectangular pulses with different maximal amplitude and finally performed experiments with a pulse amplitude corresponding to the nutation frequency of 5 Hz, which is about 10 times smaller than the distance between the lines in the NMR spectrum. As expected, the Gaussian pulse provided a better excitation selectivity as compared to the equivalent rectangular pulse: one can see that the Gaussian pulse did not excite the central lines of the NMR multiplet (Fig. 9c). Despite the fact that SLIC is expected to be less efficient compared to selective excitation, in experiments we observed that both methods have almost the same efficiency (close to the SLIC

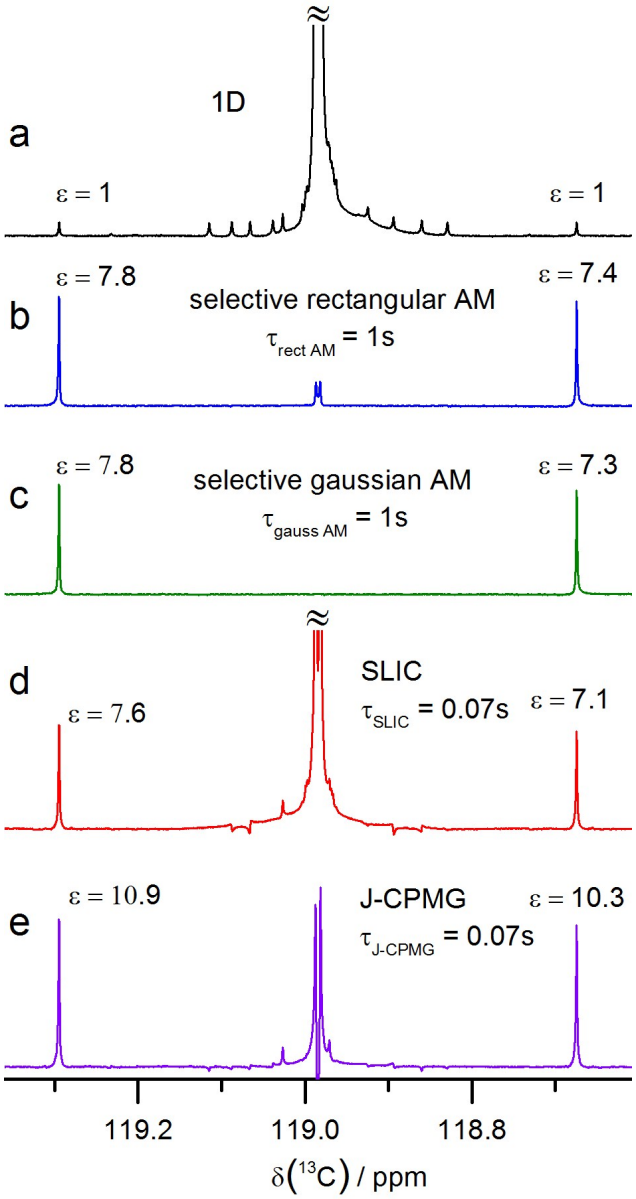

Fig. 9. Comparison of the enhancement of the OST coherences obtained with the selective AM excitation, SLIC and J-CPMG methods. (a) Standard ^{13}C NMR experiment detected at $B_0 = 16.4$ T. Numerous satellites due to minority isotopomers with additional ^{13}C nuclei are visible, as well as the small OST peaks. (b) Simultaneous selective excitation of the OST transitions by a cosine-modulated rectangular pulse with the parameters $\nu_{rf} = \nu_0$, $\nu_1 = 5$ Hz, $\tau_{sel\,AM} = 1$ s, $\nu_{AM} = 54.55$ Hz; (c) Simultaneous selective excitation by Gaussian pulse with $\nu_1 = 12$ Hz. (d) Excitation of the OST transitions by a SLIC pulse, using the following parameters: $\nu_{rf} = \nu_0$, $\nu_1 = J = 54.1$ Hz, $\tau_{SLIC} = 0.07$ s. (e) Implementation of the J-CPMG method, the experimental parameters are: $\tau_e = 4.621$ ms, $n = 8$. The total duration of the pulse sequence is $\tau_{J-\ CPMG} = 0.07$ s. SLIC and J-CPMG spectra were additionally phased to obtain purely absorptive lines for OST transitions.

theoretical maximum) of $\varepsilon \approx 7.3$ (Fig. 9d). As explained in the next section, these are losses due to B_1 inhomogeneity. SLIC-pulse also excited the central lines, which is in agreement with the theory presented here. The best enhancement of $\varepsilon \approx 10.6$ is provided by the J-CPMG technique (Fig. 9e), which is close to the theoretical maximum. The overall duration of the J-CPMG

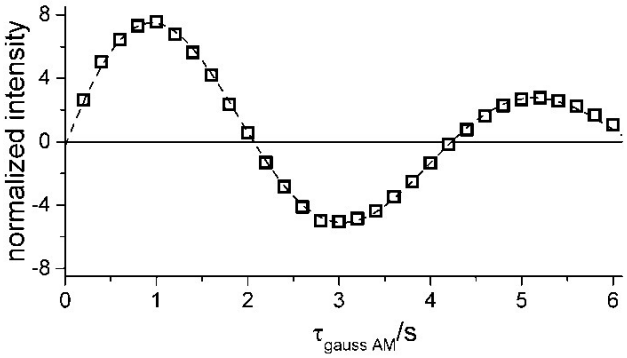

Fig. 10. Nutation curve for the OST transitions of $^{13}C_2$-**I** obtained using a cosine-modulated rectangular pulse of 5 Hz. Dashed line is a calculation with best fit parameters: $A\exp\left(\frac{\tau_{gauss\,AM}}{T_{dec}}\right)\sin\left(2\pi\,\tau_{gauss\,AM}\,\nu_1^{eff\,AM}\right)$; $A = 9.7$, $\nu_1^{eff\,AM} = 0.23$ Hz, $T_{dec} = 4.3$ s.

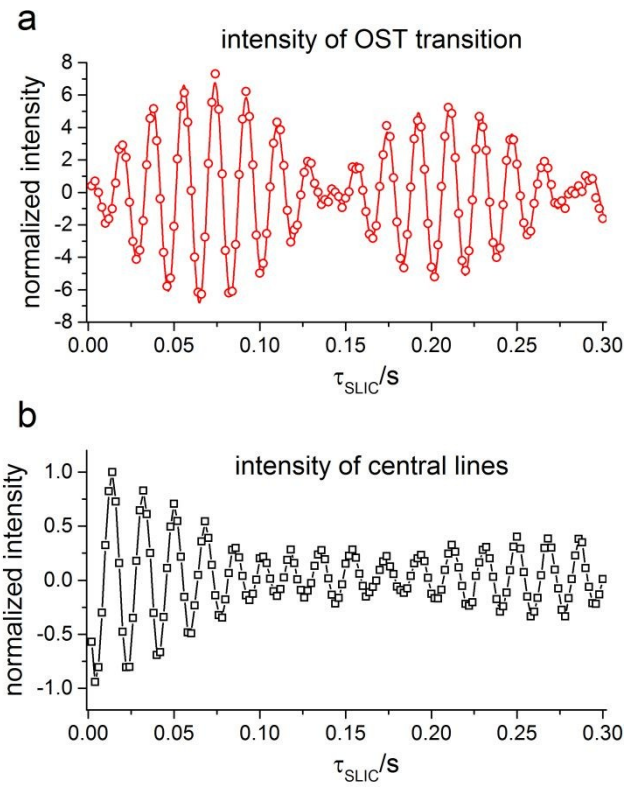

Journal Name ARTICLE

View Article Online
DOI: 10.1039/C9CP00451C

Fig. 11. Nutation patterns of the OST and triplet transitions of $^{13}C_2$-**I** under the action of a SLIC pulse. (a) Nutation of the OST transition. Solid line is a calculation with best fit parameters: $A\exp\left(\frac{\tau_{SLIC}}{T_{dec}}\right)\sin(2\pi\,\tau_{SLIC}f_1+\varphi_1)\sin(2\pi\,\tau_{SLIC}\,f_2)$; $A=7.7$, $T_{dec}=0.55$ s, $f_1=54.83$ Hz, $\varphi_1=0.4\pi$, $f_2=\frac{\Delta}{2\sqrt{2}}=3.52$ Hz. The sinal is modulated at the frequency $\frac{\Delta}{2\sqrt{2}}=3.5$ Hz, determining the optimal SLIC duration as $1/(\sqrt{2}\Delta)$ equal to 0.07 s. Normalization was performed with respect to 7.3 enhancement at 0.07 s. (b) Nutation curve for the central lines normalized with respect to central lines in a 1D spectrum.

block was the same as that for SLIC, being about 10 times shorter than the duration of the pulse used for simultaneous selective excitation. Note, that all four lines excited by J-CPMG have approximately the same intensity, which reflects the fact that the observed OST transitions had χ times bigger amplitudes but at the same time they are detected with χ

View Article Online
DOI: 10.1039/C9CP00451C

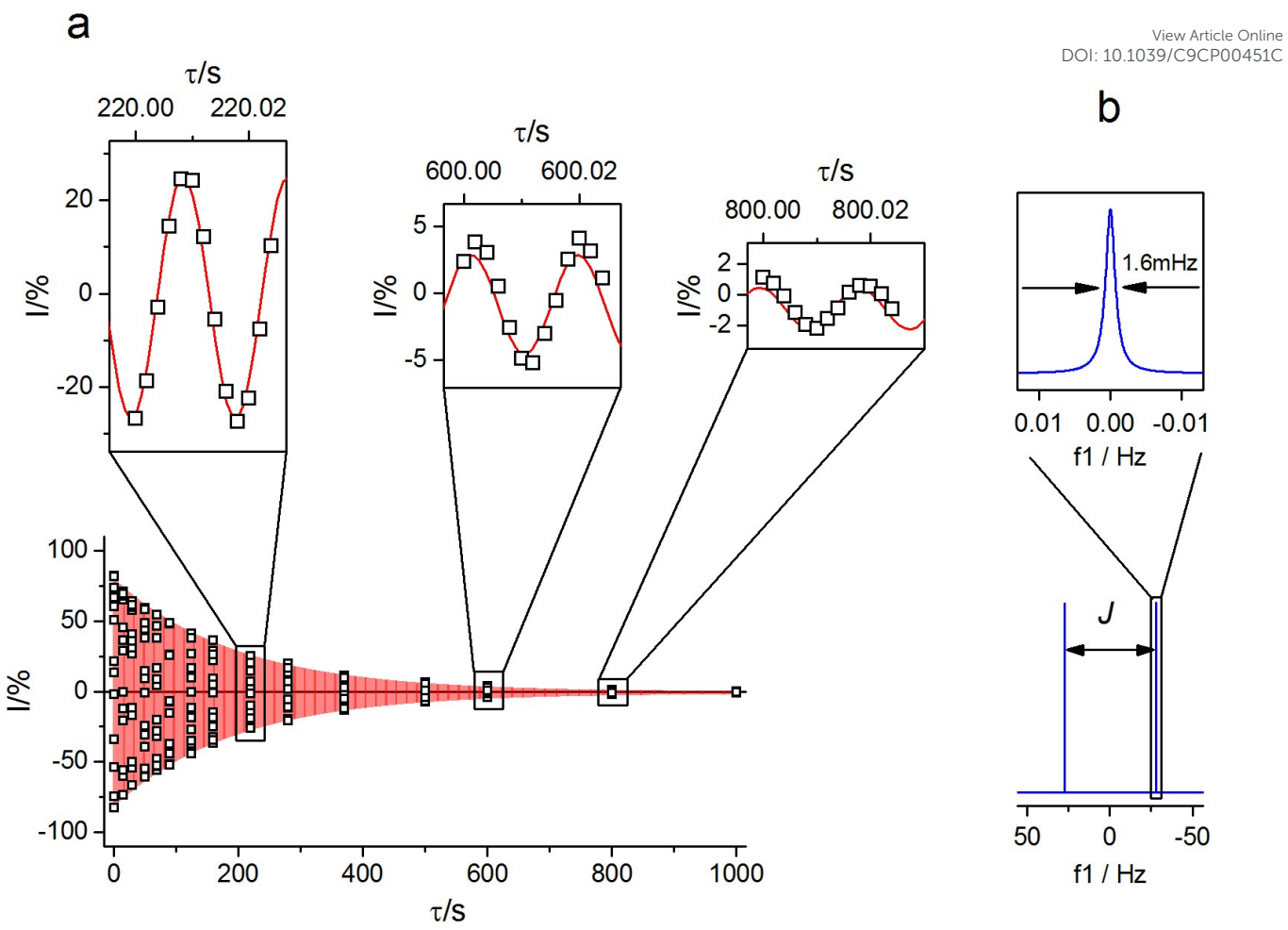

Fig. 12. (a) Time evolution of the IST coherence excited by J-CPMG at 9.4 T as a function of the residence time at the magnetic field of $B_{rel} = 5$ mT. The red line corresponds to a calculation with best fit parameters: $y_0 + A\sin(2\pi\,\tau\,\nu_{IST} + \phi)\exp\left(\frac{\tau}{T_{IST}}\right)$; $y_0 = -0.8\%$, $A = 80\%$ of thermal magnetization, $\nu_{IST} = 54.141$ Hz, $\phi = -0.7\pi$. $T_{IST} = 195$ s, longitudinal relaxation time is $T_1 = 83$ s at this B_{rel} magnetic field. Insets show data acquired around 220 s, 600 s and 800 s with the increment $\Delta\tau$ of 2 ms. Fragment of the IST coherence oscillations acquired with step $\Delta\tau = 1$ ms are shown in the insets. (b) Simulated Fourier transform of the signal corresponded to the red line in (a).

times lower efficiency than the triplet transitions. The benefit of J-CPMG is that this technique is least sensitive to ν_0 frequency and to B_1 inhomogeneities[20, 40], in the case that composite hard pulses[33] are used.

5.2 Calibration of the AM selective pulses and SLIC pulses

The dependence of the line intensity on the excitation pulse duration is termed "nutation pattern"; we acquired the nutation patterns for simultaneous selective excitation and SLIC methods (Fig. 10, 11). The nutation patterns for the central transitions, obtained using a rectangular pulse with the amplitude corresponding to $\nu_1 = 5$ Hz and a Gaussian pulse with $\nu_1 = 12$ Hz, give rise to the spin dynamics expected from theoretical consideration: spin magnetization nutates around the B_1 field with the frequency of 5 Hz.

Fig. 10 shows the nutation pattern in case of the AM rectangular pulse used for simultaneous selective excitation of the OST transitions. Purely absorptive lineshapes are observed in these experiments, when the phase of AM modulation is set according to eq. 28. The observed nutation frequency coincides with the theoretical value (see eq. 15), which is 0.23 Hz for both rectangular pulses and Gaussian pulses, so it indeed has a $\chi = 10.9$ times slower nutation frequency. We also checked that the effective nutation frequency is directly proportional to ν_1. Fitting of the nutation pattern allows one to determine precisely the efficiency of the method, removing the decay caused by B_1 inhomogeneity, which appears to be $\varepsilon = 9.7$ for rectangular and $\varepsilon =$ 10.3 for Gaussian pulses; the latter value is close to the theoretical maximum of $\varepsilon = \chi = 10.9$ in this case.

The nutation patterns obtained using a SLIC-pulse are shown in Fig. 11 for the outer peaks (Fig. 11a) and the central lines (Fig 11b). The plots almost exactly reproduce the simulated curves shown in Fig 6 for the coherence trajectories.

Hence, one can see that the SLIC-pulse first excites the coherence for an allowed transition and then a slower S-$T_{\pm 1}$ mixing takes place. The frequency of mixing equals to $\frac{\Delta}{2\sqrt{2}} = 3.5$ Hz. The central lines experience the same modulation

View Article Online
DOI: 10.1039/C9CP00451C

shifted by half period. Here fitting also reveals an effect of B_1 inhomogeneity, and the extracted amplitude reaches the maximal value expected for SLIC: $\varepsilon = 7.7$.

5.3 Excitation of the IST coherence

Having implemented the schemes for enhancing the OST transitions, we applied them for probing the IST coherence and its time dependence at low and high magnetic fields, see Fig. 12 and 13. For low field experiments, we performed field-cycling measurements by mechanical shuttling the sample from field of 9.4 T to the field, in which relaxation was studied, B_{rel}, and back. We chose $B_{rel} = 5 \pm 0.1$ mT and used the pulse sequence shown in Fig. 8b and 8c. This experiment is possible because the IST coherence frequency is almost insensitive to the B_0 field strength. More precisely, as discussed in section 2.2.2, there is a subtle B_0-dependence of the IST frequency due to the Δ-term: $\nu_{IST} = \sqrt{J^2 + \Delta^2}$, however, this results in an 0.3 Hz variation of the IST frequency at 9.4 T as compared to zero magnetic field. For this reason, it is possible to transfer the sample to a low field and back almost without any losses of the coherence amplitude and to study the IST coherence as a function of the variable residence time τ. The transfer time was kept the same, so that the IST coherence always acquired the same phase shift in each up/down shuttling. This experiment is essentially a 2D experiment, where an array of 1D spectra is acquired for a variable time τ. The oscillations in the indirect dimension last for as long as 1000 s. It was impractical to sample such a signal uniformly. For this reason, we chose 16 intervals for acquisition in the log-scale up to 1000 s; each interval contained 13 points with a fixed increment of 2 ms between them to detect a single period of a sine/cosine wave. The IST oscillation appears in the spectra as in-phase amplitude modulation of the central NMR lines. The black squares in Fig. 12 correspond to the normalized values of the integrals of the central transitions. The frequency of the oscillations can be determined very precisely being equal to $J = 54.141 \pm 0.001$ Hz; the lifetime of the coherences is $T_{IST} = 195 \pm 3$ s. At the same time, the T_1 value at the same field is $T_1 = 83$ s. Hence, the IST coherence provides approximately 2.4 -fold prolongation of the lifetime. The IST coherence generated in this way is detectable for more than 10 minutes resulting in an approximately 0.0016 Hz linewidth.

We also performed measurements at a field of 16.4 T (Fig. 13). For exciting the IST coherence, we used the pulse sequence shown in Fig. 8a, which suppresses singlet-triplet leakage. The observed relaxation time $T_{ISTx} = 6.5$ s was almost the same as $T_1 = 7.3$ s and $T_{1\rho} = 6.1$ s ($T_{1\rho}$ can be considered as a measure for T_2). Most likely, the considerably shorter T_{IST} time and T_{IST}/T_1 ratio as compared to the low-field case is due to stochastic spin interactions operative at high fields, i.e., due to the chemical shift anisotropy of the ^{13}C-nuclei. Similar results were obtained at 9.4 T magnetic field: $T_{ISTx} = 18.3$ s, $T_1 = 19.6$ s and $T_{1\rho} = 16.2$ s.

It is also informative to compare the performance of the

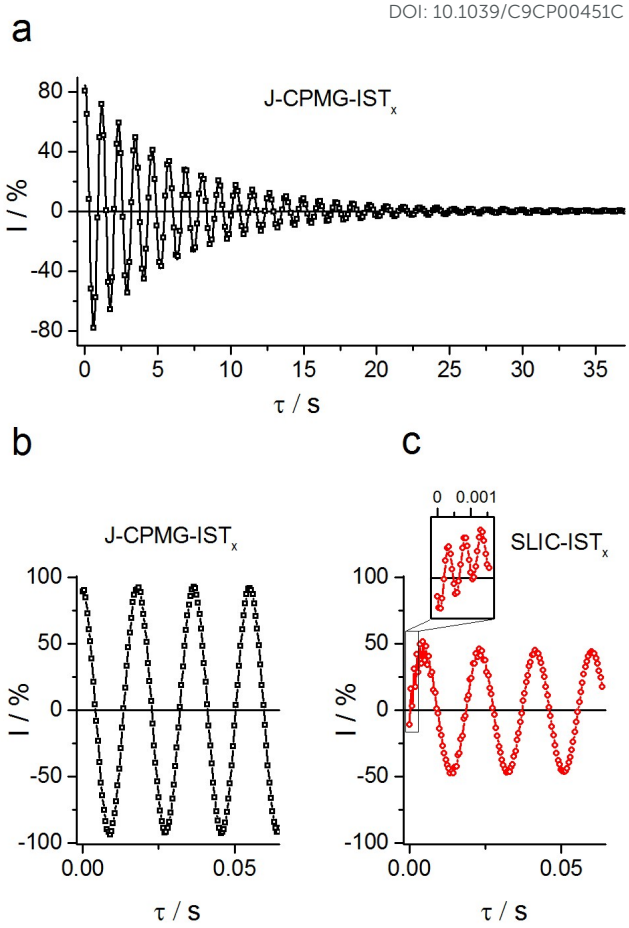

Fig. 13. (a) Time evolution of the IST$_x$ coherence. Here the magnetic field is $B_0 = 16.4$ Tesla. The distance between subsequent points in the τ-dependence $\Delta\tau$ is equal to and 145 ms $\approx \frac{8}{J}$ (a), 5 ms (b) and (c) and 0.1 ms for inset in (c). The relaxation time of the IST coherence in this case was $T_{IST} = 6.5$ s, which is close to the $T_1 = 7.3$ s value, the amplitude of the oscillations was 91.3% for J-CPMG and 49.5% for SLIC, as measured in units of thermal magnetization.

J-CPMG and SLIC methods. One can readily see that the amplitude of oscillations in the SLIC case is about two times smaller, resulting from two subsequent transformations with the efficiency of $\frac{1}{\sqrt{2} * \sqrt{2}} = 0.5$. This result is in agreement with our estimates of the efficiency of generating the OST coherence of 100% for J-CPMG and 70% for SLIC.

As discussed in section 2.1.3, the SLIC-pulse also excites single quantum coherences. They manifest themselves in fast oscillations which are observed at short delays having the frequency corresponding to the amplitude of the spin-locking field, which was here 1 kHz (Fig. 13c). The IST$_x$ evolution frequency is 54.15 Hz for both methods. We also performed the IST$_z$ experiment (Fig. 4b) and obtained the relaxation time of $T_{ISTz} = 7.1$ s and the oscillation frequency of 55.12 Hz equal to $\sqrt{J^2 + \Delta^2}$. Hence, we were able to generate the IST coherences using simultaneous selective excitation (here are not shown),

SLIC and J-CPMG elements and demonstrated the long-lived nature of the coherence under the study.

6 Conclusions

In this work, we propose NMR techniques for manipulating spin order in strongly coupled spin pairs. Specifically, we examined methods for enhancing weak NMR transitions by efficient excitation of the corresponding OST coherences. These methods have been implemented for the molecule containing pair of nearly equivalent ^{13}C spins although the schemes are more general and can be applied to more complex spin systems such as $AA'XX'$, $AA'(XX')_2$, etc. The proposed techniques can be useful for generating and probing long-lived spin order and for determining *J*-couplings with high accuracy.

All the methods for enhancement of the OST coherences can be used in pulse sequences to probe the evolution of the IST coherence; we have found the J-CPMG technique to be the most robust and efficient method. We would like to stress that the IST coherence is probed by measuring the intensity of the central "allowed" NMR transitions (not the weak satellites) by monitoring quantum oscillations upon variation of the IST evolution time τ. High amplitude of such oscillations is a clear indication of the high magnetization-to-IST-to-magnetization efficiency that we can achieve. The frequency of the IST coherences is almost independent of the magnetic field; thus the IST coherence is immune to field inhomogeneity, allowing to vary the external magnetic field during the experiment and to use the pulsed field gradients to filter out other spin coherences. We have found that for the compound under study at high fields the IST coherence has approximately the same lifetime as the longitudinal relaxation time, whereas at low fields the IST lifetime is equal to $2.4 \cdot T_1$.

Conflicts of interest

There are no conflicts to declare.

Acknowledgements

Novosibirsk team acknowledges support from the Russian Science Foundation (grant No. 19-43-04116) and Ministry of Science and Higher Education of the Russian Federation for providing access to NMR facilities. The Southampton group acknowledges support from EPSRC (grant numbers EP/N002482/1, EP/P009980, EP/P030491/1, EP/P005187/1).

References

1 M. Carravetta, O. G. Johannessen and M. H. Levitt, *Phys. Rev. Lett.*, 2004, 92, 153003.
2 M. Carravetta and M. H. Levitt, *J. Am. Chem. Soc.*, 2004, 126, 6228-6229.
3 M. H. Levitt, in *Annu. Rev. Phys. Chem.*, eds. M. A. Johnson and T. J. Martinez, Annual Reviews, Palo Alto, 2012, 63, 89-105.
4 G. Pileio, *Prog. Nucl. Magn. Reson. Spectrosc.*, 2017, 98–99, 1-19.
5 P. Ahuja, R. Sarkar, S. Jannin, P. R. Vasos and G. Bodenhausen, *Chem. Commun.*, 2010, 46, 8192-8194.
6 P. R. Vasos, A. Comment, R. Sarkar, P. Ahuja, S. Jannin, J. P. Ansermet, J. A. Konter, P. Hautle, B. Van Den Brandt and G. Bodenhausen, *Proc. Natl. Acad. Sci. U. S. A.*, 2009, 106, 18469-18473.
7 G. Pileio, S. Bowen, C. Laustsen, M. C. D. Tayler, J. T. Hill-Cousins, L. J. Brown, R. C. D. Brown, J. H. Ardenkjaer-Larsen and M. H. Levitt, *J. Am. Chem. Soc.*, 2013, 135, 5084-5088.
8 M. C. D. Tayler, I. Marco-Rius, M. I. Kettunen, K. M. Brindle, M. H. Levitt and G. Pileio, *J. Am. Chem. Soc.*, 2012, 134, 7668-7671.
9 A. Bornet, P. Ahuja, R. Sarkar, L. Fernandes, S. Hadji, S. Y. Lee, A. Haririnia, D. Fushman, G. Bodenhausen and P. R. Vasos, *ChemPhysChem*, 2011, 12, 2729-2734.
10 R. Sarkar, P. R. Vasos and G. Bodenhausen, *J. Am. Chem. Soc.*, 2007, 129, 328-334.
11 P. Ahuja, R. Sarkar, P. R. Vasos and G. Bodenhausen, *J. Am. Chem. Soc.*, 2009, 131, 7498-7499.
12 J. N. Dumez, J. T. Hill-Cousins, R. C. D. Brown and G. Pileio, *J. Magn. Reson.*, 2014, 246, 27-30.
13 R. Buratto, D. Mammoli, E. Chiarparin, G. Williams and G. Bodenhausen, *Angew. Chem., Int. Ed.*, 2014, 53, 11376-11380.
14 N. Salvi, R. Buratto, A. Bornet, S. Ulzega, I. R. Rebollo, A. Angelini, C. Heinis and G. Bodenhausen, *J. Am. Chem. Soc.*, 2012, 134, 11076-11079.
15 G. Pileio, M. Carravetta and M. H. Levitt, *Phys. Rev. Lett.*, 2009, 103, 083002.
16 A. Bornet, R. Sarkar and G. Bodenhausen, *J. Magn. Reson.*, 2010, 206, 154-156.
17 R. Sarkar, P. Ahuja, P. R. Vasos and G. Bodenhausen, *Phys. Rev. Lett.*, 2010, 104, 053001.
18 R. Sarkar, P. Ahuja, P. R. Vasos, A. Bornet, O. Wagnieres and G. Bodenhausen, *Prog. Nucl. Magn. Reson. Spectrosc.*, 2011, 59, 83-90.
19 A. Bornet, S. Jannin, J. A. Konter, P. Hautle, B. van den Brandt and G. Bodenhausen, *J. Am. Chem. Soc.*, 2011, 133, 15644-15649.
20 M. C. D. Tayler and M. H. Levitt, *Phys. Chem. Chem. Phys.*, 2011, 13, 5556-5560.
21 G. Stevanato, J. T. Hill-Cousins, P. Hakansson, S. S. Roy, L. J. Brown, R. C. D. Brown, G. Pileio and M. H. Levitt, *Angew. Chem., Int. Ed.*, 2015, 54, 3740-3743.
22 G. Pileio, J. T. Hill-Cousins, S. Mitchell, I. Kuprov, L. J. Brown, R. C. D. Brown and M. H. Levitt, *J. Am. Chem. Soc.*, 2012, 134, 17494-17497.
23 K. F. Sheberstov, H.-M. Vieth, H. Zimmermann, K. L. Ivanov, A. S. Kiryutin and A. V. Yurkovskaya, *Appl. Magn. Reson.*, 2018, 49, 293-307.
24 S. J. DeVience, R. L. Walsworth and M. S. Rosen, *Phys. Rev. Lett.*, 2013, 111.
25 T. Theis, Y. Feng, T. Wu and W. S. Warren, *J. Chem. Phys.*, 2014, 140.
26 M. H. Levitt, *Spin dynamics: basics of nuclear magnetic resonance,* 2nd ed., 2008.
27 J. A. Pople, *High-resolution nuclear magnetic resonance*, McGraw-Hill, New York,, 1959.
28 H. Günther, *NMR spectroscopy : basic principles, concepts, and applications in chemistry*, Wiley, Chichester ; New York, 3rd ed., 2013.
29 O. W. Sørensen, *J. Magn. Reson.*, 1990, 86, 435-440.
30 M. H. Levitt, *J. Magn. Reson.*, 2016, 262, 91-99.
31 H. Y. Carr and E. M. Purcell, *Phys. Rev.*, 1954, 94, 630-638.
32 S. Meiboom and D. Gill, *Rev. Sci. Instrum.*, 1958, 29, 688-691.
33 M. H. Levitt, *Prog. Nucl. Magn. Reson. Spectrosc.*, 1986, 18, 61-122.

Journal Name ARTICLE

View Article Online
DOI: 10.1039/C9CP00451C

34 M. Leskes, P. K. Madhu and S. Vega, *Prog. Nucl. Magn. Reson. Spectrosc.*, 2010, 57, 345-380.
35 Y. Zur, M. H. Levitt and S. Vega, *J. Chem. Phys.*, 1983, 78, 5293-5310.
36 Y. Zur and S. Vega, *J. Chem. Phys.*, 1983, 79, 548-558.
37 S. Vega, *J. Chem. Phys.*, 1978, 68, 5518-5527.
38 J. T. Hill-Cousins, I. A. Pop, G. Pileio, G. Stevanato, P. Hakansson, S. S. Roy, M. H. Levitt, L. J. Brown and R. C. D. Brown, *Org. Lett.*, 2015, 17, 2150-2153.
39 T. M. Barbosa, R. Rittner, C. F. Tormena, G. A. Morris and M. Nilsson, *RSC Adv.*, 2016, 6, 95173-95176.
40 B. Kharkov, X. Duan, J. W. Canary and A. Jerschow, *J. Magn. Reson.*, 2017, 284, 1-7.
41 A. S. Kiryutin, A. V. Yurkovskaya, H. Zimmermann, H.-M. Vieth and K. L. Ivanov, *Magn. Reson. Chem.*, 2018, 56, 651-662.
42 I. V. Zhukov, A. S. Kiryutin, A. V. Yurkovskaya, Y. A. Grishin, H.-M. Vieth and K. L. Ivanov, *Phys. Chem. Chem. Phys.*, 2018, 20, 12396-12405.
43 C. Rischel, *J Magn Reson Ser A*, 1995, 116, 255-258.
44 C. Bengs and M. H. Levitt, *Magn. Reson. Chem.*, 2018, 56, 374-414.
45 D. A. Cheshkov, K. F. Sheberstov, D. O. Sinitsyn and V. A. Chertkov, *Magn. Reson. Chem.*, 2018, 56, 449-457.